PERGAMON

International Journal of Multiphase Flow 28 (2002) 105–125

International Journal of Multiphase Flow

www.elsevier.com/locate/ijmulflow

Effects of magnetic field on the shape of a bubble in a uniaxial straining flow

S.M. Shin, I.S. Kang *

Department of Chemical Engineering/Division of Mechanical and Industrial Engineering, Pohang University of Science and Technology, San 31, Hyoja-dong, Nam-gu, Pohang 790-784, South Korea

Received 1 October 2000; received in revised form 1 September 2001

Abstract

In some processes such as the Liquid Metal MagnetoHydroDynamic (LMMHD) generator, an inert gas is blown into an electrically conducting fluid to control the behavior of the liquid metal in a magnetic field. In the present work, the effects of magnetic field on the deformation and breakup of a bubble in a uniaxial straining flow of conducting fluid are investigated by using the numerical analysis. Specifically, the steady bubble shape is first determined as a function of three dimensionless parameters: the Reynolds number (Re), the Weber number (W), and the magnetic interaction parameter (N). Then, the critical phenomena such as bubble breakup are studied based on the concept of existence of steady solutions. Finally, a full unsteady numerical code is adopted for verification of the critical phenomena in the bubble dynamics. In all computations, as a reference, the far field velocity distribution is assumed to be fixed. From the numerical results, it is found that the steady bubble deformation increases with the strength of the magnetic field for small N. When N is increased further with fixed Re and W, the bubble shows distinct deformation characteristics depending on the value of W. If W is larger than a certain threshold value (W_{th}), there exists a critical range of N, $N_{c1}(W) < N < N_{c2}(W)$, for which no converged steady-state solution has been obtained. However, if $W < W_{th}$, the steady bubble deformation increases monotonously with the increase of N and no such a critical phenomenon has been observed. Unsteady numerical analysis shows that a bubble extends indefinitely in the critical range of the parameters found by the steady analysis. Based on the numerical results, the diagram for stability and breakup is prepared for a bubble in a linear flow of conducting fluid under magnetic field. The diagram is expected to provide a valuable information on the bubble size estimation which is essential in two-phase flow modeling.

Keywords: Bubble deformation; Bubble breakup; Uniaxial flow; Magnetic field; Liquid metal–gas flow; Stability diagram

* Corresponding author. Tel.: +82-54-279-2273; fax: +82-54-279-2699.
E-mail address: iskang@postech.ac.kr (I.S. Kang).

0301-9322/02/$ - see front matter
PII: S0301-9322(01)00063-5

1. Introduction

One of the interesting problems in the study of bubbly flows is the estimation of the size and shape of a bubble under external fields such as an electric or a magnetic field. This problem lies at the core in various applications. In the case of electric field application (e.g. EHD problem), most fluids are transparent and it is easy to observe the behavior of a bubble (Jones, 1978; Cho et al., 1996). Thus, there have been many experimental and theoretical works on the effect of electric field on the behavior of bubbly flow. However, in the case of magnetic field application (e.g. MHD problem), most electrically conducting fluids are opaque and it is difficult to observe the behavior of a bubble in such systems. Due partly to the experimental difficulties, the theoretical works on this problem have also been retarded. Nonetheless, the bubbly flows play important roles in the design of energy conversion and material processing systems and they should be analyzed appropriately. In the present paper, therefore, we are concerned with the behavior of a single bubble in an electrically conducting fluid under the magnetic field as a preliminary step for the researches in this direction.

The present problem has its relevance to several practically important applications. We can find number of situations in which two-phase flows of a gas and a conducting liquid play important roles. Such processes include the Liquid Metal MagnetoHydroDynamic (LMMHD) generator system. The two-phase fluid in LMMHD consists of a mixture of an electrodynamic fluid (a liquid metal) and a thermodynamic fluid (a gas such as helium). The thermodynamic fluid expands as it passes through the divergent channel and carries the electrodynamic fluid along with it.

In the modeling of two-phase flow system, it is of great importance to estimate the average size of the bubbles in the system. Since the deformation and breakup of a bubble is mainly due to the rate of strain of the local flow field around the bubble, the dynamics of a bubble in a straining flow has been studied extensively. However, the analysis thus far has been limited mostly to the cases without electromagnetic field effects.

For the plain two-phase flow without electromagnetic field effects, most investigators have assumed the existence of a critical Weber number (W_c) based upon the dimensional analysis without any detailed information on the critical value. The first major contribution to the bubble breakup theory was made by the numerical works of Miksis (1981) and Ryskin and Leal (1984b) on the finite deformation of a bubble in a uniaxial straining flow. Miksis considered the bubble breakup in the inviscid case and concluded that no steady solution exists for the Weber number (W) beyond a maximum critical value, W_c. Ryskin and Leal studied steady bubble deformation for non-zero viscosity cases. Ryskin and Leal used an iterative method to solve the full steady-state Navier–Stokes equations for a series of finite values of the Reynolds number (Re) with $Re = \infty$ case as a limiting value. In their numerical works, they could obtain steady bubble shapes only for the Weber numbers less than the critical values, beyond which no converged solution could be obtained. Later, Kang and Leal (1987) used a full time-dependent numerical scheme to study the problem of unsteady bubble deformation in a uniaxial straining flow at several Reynolds numbers (including $Re = \infty$). By showing explicitly that a bubble is elongated indefinitely if the Weber number is larger than the critical value, they verified that the critical values predicted by Ryskin and Leal are the true critical values for the existence of steady solutions. In addition, the unsteady analysis on the bubble dynamics revealed many interesting nonlinear dynamical characteristics of a bubble in straining flows.

As we have seen above, the bubble dynamics in straining flows have been studied extensively. However, there has been no systematic analysis on the breakup of a bubble in an electrically conducting fluid under magnetic field. This fact provides the first motivation of the present work. When the magnetic field is applied, we need to consider another important dimensionless parameter in addition to the Reynolds number (Re) and the Weber number (W). That is the magnetic interaction parameter, denoted by N, which represents the effect of the magnetic field. Therefore, the objectives of the present work can be summarized as follows. If there exists a critical Weber number, we want to predict it as a function of the Reynolds number and the magnetic interaction parameter, i.e. $W_c = W_c(Re, N)$. In addition, we want to obtain the information on bubble shapes at subcritical Weber numbers, i.e. Shape $= f(Re, N, W)$ for $W < W_c$. The goal of the present work will be achieved by extending previous numerical works on the bubble dynamics in straining flows, especially the works of Ryskin and Leal (1984b) and Kang and Leal (1987).

Before going on to the main part of the paper, we need to mention the recent works of Eckert et al. (2000a,b). They considered the behavior of gas bubbles in a turbulent metal magnetohydrodynamic flow. They studied the influence of the magnetic field on the bubble dispersion and the slip ratio. They used one-dimensional model and compared the computational results with the experimental results. In their model, the bubble radius is an important parameter and the value has been assumed for the analysis. Since our work is aimed to provide a valuable information on the bubble size estimation, the results in this paper are expected to be useful for the researchers such as Eckert et al.

2. Statement of the problem

We consider deformation of an incompressible gas bubble of volume $(4/3)\pi a_0^3$ in an axisymmetric straining flow under a uniform magnetic field applied in x-direction as shown in Fig. 1. The

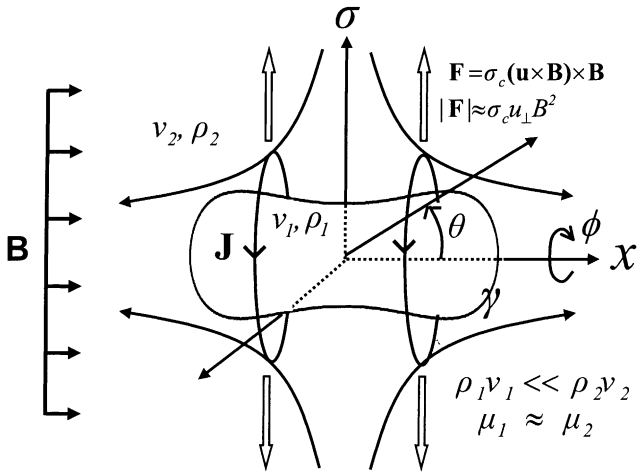

Fig. 1. A bubble in a linear flow of a conducting fluid under magnetic field.

density and viscosity of the gas inside the bubble are assumed to be negligible in comparison with those of the liquid ($\rho_1 \ll \rho_2$, $\rho_1 v_1 \ll \rho_2 v_2$). Both the gas and the liquid are assumed to be non-magnetizable, and thus the magnetic permeability of both phase are almost the same, $\mu_1 \simeq \mu_2$. The density and the viscosity of the external fluid are assumed to be constant. Furthermore, the surface of the bubble is assumed to be characterized by a uniform surface tension γ. We neglect all the effects of gravity including the hydrostatic pressure variation in the fluid. The dimensional velocity field far from the bubble is assumed to be given by the uniaxial straining flow, which can be represented in the Cartesian coordinates by

$$\tilde{\mathbf{u}}_\infty = \tilde{\mathbf{E}} \cdot \tilde{\mathbf{x}}, \quad \tilde{\mathbf{E}} = E_0 \begin{pmatrix} 1 & 0 & 0 \\ 0 & -\frac{1}{2} & 0 \\ 0 & 0 & -\frac{1}{2} \end{pmatrix}, \quad E_0 > 0, \tag{1}$$

where E_0 is the principal strain rate.

The governing equations for the fluid motion are the continuity equation and the equation of motion:

$$\tilde{\nabla} \cdot \tilde{\mathbf{u}} = 0, \tag{2}$$

$$\left(\frac{\partial \tilde{\mathbf{u}}}{\partial \tilde{t}} + \tilde{\mathbf{u}} \cdot \tilde{\nabla} \tilde{\mathbf{u}} \right) = -\frac{1}{\rho} \tilde{\nabla} \tilde{p} + \nu \widetilde{\nabla^2} \tilde{\mathbf{u}} + \frac{1}{\rho} (\tilde{\mathbf{J}} \times \tilde{\mathbf{B}}), \tag{3}$$

where $\tilde{\mathbf{J}}$ is the induced current and $\tilde{\mathbf{B}}$ is the magnetic induction. The equation of magnetic field for a linear, isotropic, and homogeneous material is represented as

$$\frac{\partial \tilde{\mathbf{B}}}{\partial \tilde{t}} - \tilde{\nabla} \times (\tilde{\mathbf{u}} \times \tilde{\mathbf{B}}) = \frac{1}{\mu \sigma_c} \widetilde{\nabla^2} \tilde{\mathbf{B}}, \tag{4}$$

where μ is the magnetic permeability and σ_c is the electrical conductivity.

For the boundary conditions, we have

$$\tilde{\mathbf{u}} \to \tilde{\mathbf{E}} \cdot \tilde{\mathbf{x}} \quad \text{as} \quad \tilde{\mathbf{x}} \to \infty \tag{5}$$

as the far field condition. At the bubble surface, we have:

- *Kinematic condition*

$$\frac{1}{|\tilde{\nabla} \tilde{F}|} \frac{\partial \tilde{F}}{\partial \tilde{t}} + \tilde{\mathbf{u}} \cdot \mathbf{n} = 0. \tag{6}$$

- *Normal stress condition*

$$[|\mathbf{n} \cdot (\mathbf{n} \cdot \tilde{\mathbf{T}})|] = \gamma \tilde{\nabla} \cdot \mathbf{n}. \tag{7}$$

- *Tangential stress condition*

$$[|\mathbf{t} \cdot (\mathbf{n} \cdot \tilde{\mathbf{T}})|] = 0. \tag{8}$$

- *Magnetic field condition*

$$\tilde{B}_{1n} = \tilde{B}_{2n}, \tag{9}$$

$$\tilde{H}_{1t} = \tilde{H}_{2t}. \tag{10}$$

In the above, $\tilde{F}$ is the shape function that describes the bubble shape as $\tilde{F}(\tilde{\mathbf{x}}, \tilde{t}) = 0$. $[|\cdot|]$ in the normal stress condition and the tangential stress condition denotes the difference of the quantity between the outside and inside phases. In (9) and (10), $\mathbf{B} = \mu\mathbf{H}$ and the subscripts n and t denote the normal and the tangential components. In addition to the above boundary conditions, the bubble shape must satisfy the constraint of volume conservation $V = V_0 = (4/3)\pi a_0^3$.

To non-dimensionalize the governing equations and the boundary conditions, we introduce the characteristic scales:

$$l_c = a_0, \quad u_c = E_0 a_0, \quad p_c = \rho u_c^2, \quad t_c = \frac{1}{E_0}, \quad B_c = B_0,$$

where a_0 is the radius of the equivalent spherical bubble, and B_0 the magnitude of the applied uniform magnetic field. Then the governing equations for the fluid motion become

$$\nabla \cdot \mathbf{u} = 0, \tag{11}$$

$$\left(\frac{\partial \mathbf{u}}{\partial t} + \mathbf{u} \cdot \nabla \mathbf{u}\right) = -\nabla p + \frac{1}{Re}\nabla^2 \mathbf{u} + N(\mathbf{J} \times \mathbf{B}), \tag{12}$$

where Re and N are the Reynolds number and the magnetic interaction parameter defined by

$$Re = \frac{E_0 a_0^2}{\nu} \quad \text{and} \quad N = \frac{\sigma_c B_c^2}{\rho E_0}. \tag{13}$$

The dimensionless magnetic field equation is

$$\frac{\partial \mathbf{B}}{\partial t} - \nabla \times (\mathbf{u} \times \mathbf{B}) = \frac{1}{Re_m}\nabla^2 \mathbf{B}, \tag{14}$$

where Re_m is the magnetic Reynolds number defined as $Re_m = \mu\sigma_c u_c l_c$. In the present work, we assume that $Re_m \ll 1$. For a typical case of a molten metal on the laboratory scale of $\mu\sigma_c \simeq 1\ \mathrm{m^{-2}\ s}$, $u_c \simeq 10^{-1}\ \mathrm{m\ s^{-1}}$, and $l_c \simeq 10^{-2}\ \mathrm{m}$, we have $Re_m \simeq 10^{-3}$ and our assumption is valid. In this situation the magnetic field equation is simplified to

$$\nabla^2 \mathbf{B} = 0. \tag{15}$$

It is assumed that the magnetic permeabilities are the same for both phases. Furthermore, as the far field condition, we have the uniform magnetic field condition. Therefore, the magnetic field is simply given by the uniform field

$$\mathbf{B} = \mathbf{e}_x \tag{16}$$

everywhere.

3. Preliminary analysis

Before performing the detailed numerical analysis, some preliminary steps are taken for better understanding of the problem.

3.1. The Lorentz force

The induced current is given in dimensional form by (Moreau, 1990)

$$\tilde{\mathbf{J}} = \sigma_c(\tilde{\mathbf{E}} + \tilde{\mathbf{u}} \times \tilde{\mathbf{B}}). \tag{17}$$

At steady state, Faraday's law states

$$\tilde{\nabla} \times \tilde{\mathbf{E}} = -\frac{\partial \tilde{\mathbf{B}}}{\partial \tilde{t}} = \mathbf{0}. \tag{18}$$

Therefore, the electric field can be represented as $\tilde{\mathbf{E}} = -\tilde{\nabla}\tilde{\phi}$. From $\nabla \cdot \tilde{\mathbf{J}} = 0$, we have for the uniform magnetic field case

$$\widetilde{\nabla^2}\tilde{\phi} = \tilde{\nabla} \cdot (\tilde{\mathbf{u}} \times \tilde{\mathbf{B}}) = \tilde{\mathbf{B}} \cdot \tilde{\boldsymbol{\omega}}, \tag{19}$$

where $\tilde{\boldsymbol{\omega}} = \tilde{\nabla} \times \tilde{\mathbf{u}}$ is the vorticity vector.

We now can show that if the applied magnetic field is parallel to the axis of symmetry, the resulting Lorentz force is also axisymmetric and the whole problem can be an axisymmetric problem. However, if the applied magnetic field is not parallel to the symmetry axis, the Lorentz force is not axisymmetric and the axisymmetry assumption may not be used.

When the magnetic field is parallel to the rotation axis, we have $\tilde{\mathbf{B}} = B_0\mathbf{e}_x$ while the vorticity is given by $\tilde{\boldsymbol{\omega}} = \tilde{\omega}\mathbf{e}_\phi$ for the axisymmetric flow field. Therefore, we have $\tilde{\mathbf{B}} \cdot \tilde{\boldsymbol{\omega}} = 0$ and $\widetilde{\nabla^2}\tilde{\phi} = 0$. Since the bubble surface is insulating and the induced current should form a closed path, both at the bubble surface and far away from the bubble we have $\mathbf{n} \cdot \tilde{\mathbf{J}} = 0$. Therefore, we have

$$\mathbf{n} \cdot \tilde{\mathbf{J}} = \sigma_c\left(-\frac{\partial \tilde{\phi}}{\partial n} + \mathbf{n} \cdot (\tilde{\mathbf{u}} \times \tilde{\mathbf{B}}) \right) = 0. \tag{20}$$

Since for the axisymmetric flow field $\tilde{\mathbf{u}} \times \tilde{\mathbf{B}} = \|\tilde{\mathbf{u}} \times \tilde{\mathbf{B}}\|\mathbf{e}_\phi$, we have $\mathbf{n} \cdot (\tilde{\mathbf{u}} \times \tilde{\mathbf{B}}) = 0$. Therefore, $\partial\tilde{\phi}/\partial n = 0$ both at the bubble surface and far away from the bubble. Thus $\tilde{\phi} = \text{const}$ and $\tilde{\mathbf{E}} = -\tilde{\nabla}\tilde{\phi}$ should vanish. In this case, the Lorentz force is simplified to

$$\tilde{\mathbf{F}}_L = \sigma_c(\tilde{\mathbf{u}} \times \tilde{\mathbf{B}}) \times \tilde{\mathbf{B}} = -(\tilde{u}_y\mathbf{e}_y + \tilde{u}_z\mathbf{e}_z)B_0^2 \tag{21}$$

and it is axisymmetric. The Lorentz force distribution is shown in Fig. 1.

As mentioned previously, it should be kept in mind that, if the applied magnetic field is not parallel to the rotation axis, the whole problem may not be axisymmetric any more. In that case, a full three-dimensional analysis should be performed.

3.2. Effect of magnetic field on the pressure field of undisturbed straining flow

When the magnetic field is in the x-direction, the dimensionless governing equation becomes

$$\frac{\partial \mathbf{u}}{\partial t} + \mathbf{u} \cdot \nabla\mathbf{u} = -\nabla p + \frac{1}{Re}\nabla^2\mathbf{u} - N(u_y\mathbf{e}_y + u_z\mathbf{e}_z). \tag{22}$$

The far field velocity is given as

$$\mathbf{u}_\infty = \mathbf{E}\cdot\mathbf{x} = \left(x, -\frac{y}{2}, -\frac{z}{2}\right). \tag{23}$$

By substituting the above velocity distribution to the governing equation, we have

$$p = p_0 - \frac{1}{2}x^2 + \left(N - \frac{1}{2}\right)\left[\left(\frac{y}{2}\right)^2 + \left(\frac{z}{2}\right)^2\right]. \tag{24}$$

The pressure distributions for the cases of $N = 0$ and $N > 0.5$ are shown in Fig. 2, where σ is the radial coordinate of the cylindrical coordinate system and $\sigma = (y^2 + z^2)^{1/2}$. As shown in the figure, the far field pressure distribution must be changed to maintain the same velocity field under the magnetic field. Since

$$\mathbf{F}_L \cdot \mathbf{u} = -N(u_y^2 + u_z^2) < 0, \tag{25}$$

the fluid loses its energy due to the magnetic field. In order to compensate this loss, the pressure field must be changed as shown in the figure.

At this point a remark should be made to the far field condition. In this work, we are concerned with the effect of magnetic field on the bubble behavior of deformation and breakup under the condition that the far field velocity distribution is fixed. The problem defined in this way can find its relevance to the *macroscopic* modeling of real bubbly flows as follows. Of course, when a bubbly flow is subjected to magnetic field, the mean flow around a bubble may

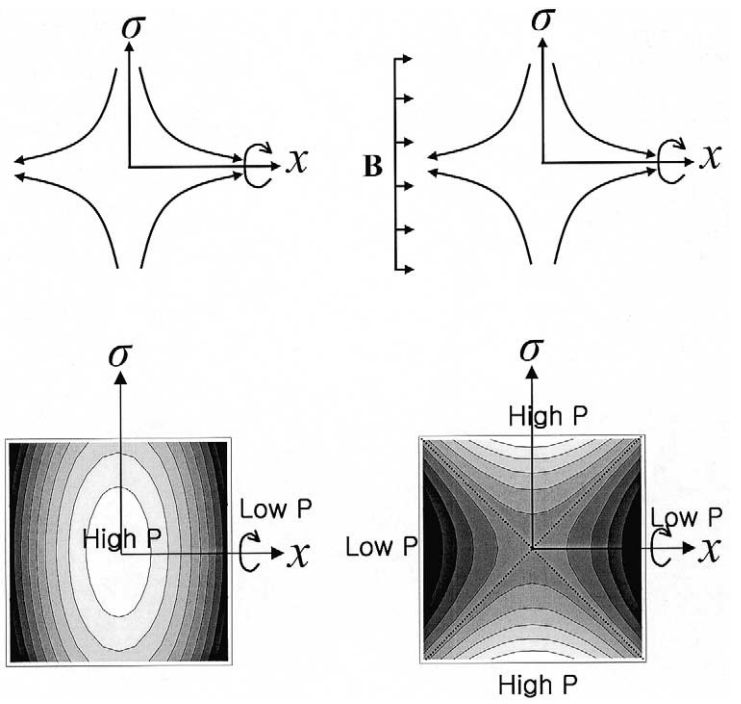

Fig. 2. The pressure distributions in the uniaxial straining flow in the cases with and without magnetic field.

be changed due to the action of magnetic field. Nevertheless, in terms of relative velocity, the mean flow around a bubble can be regarded as a linear flow with a certain rate of strain, which is a function of the applied magnetic field and other factors. Here we should recognize that it is determined from the overall macroscopic problem of the bubbly flow. On the other hand, however, the overall bubbly flow is influenced by the microscopic bubble behavior. Thus the prediction of bubble behavior based on the *microscopic* analysis is essential for any successful *macroscopic* modeling of bubbly flow. The procedure of the overall modeling of bubbly flow under magnetic field will be like the following. First, by solving the macroscopic problem, we determine the flow field under the magnetic field and the distribution of the local rate of strain. Then for each point, the local rate of strain determined from the macroscopic problem is used to determine the far field condition for the microscopic analysis. This microscopic analysis of the bubble behavior under magnetic field produces the information on breakup and deformation (the present work is for this microscopic part). That information is used for the prediction of rheological properties of the macroscopic flow. In this way, we can analyze the bubbly flow by iterating these steps several times.

The analysis of the present study may seem to be in a very limited scope in the sense that the magnetic field is parallel to the rotation axis of an axisymmetric bubble. In general, the local linear flow is not necessarily axisymmetric and the magnetic field is not necessarily parallel to the rotation axis of a deformed bubble. However, it is emphasized that all these assumptions have been made to make the problem as simple as possible, while the main ingredient of the analysis is kept.

4. Numerical scheme

As mentioned before in Section 1, the present work is related to the previous works of Ryskin and Leal (1984a,b), and Kang and Leal (1987). The former work is about the steady solution of the bubble shape in a uniaxial straining flow, and the latter is its unsteady version. In the present work, we include the Lorentz force term to study the effects of magnetic field on the bubble deformation and breakup. Therefore, we have closely followed the numerical scheme of Kang and Leal. In the following, the brief summary of the scheme is presented.

In order to follow the bubble deformation, we have used the boundary-fitted curvilinear coordinate system which was originally developed by Ryskin and Leal (1983). One example is shown in Fig. 3, where the original coordinate variables x and σ of the cylindrical coordinate system are mapped by the relations

$$x = x(\xi, \eta), \quad \sigma = \sigma(\xi, \eta). \tag{26}$$

In the present problem, we have used the symmetries and we have considered only the region of $0 \leqslant \theta \leqslant (\pi/2)$. In the coordinate system, $\xi = 1$ corresponds to the bubble surface and $\xi = 0$ to the points at infinity. The coordinate line $\eta = 0$ corresponds to the rotation axis while $\eta = 1$ corresponds to the equatorial plane.

The governing equations for the fluid motion (Eqs. (11) and (12)) were reformulated in terms of streamfunction and vorticity as

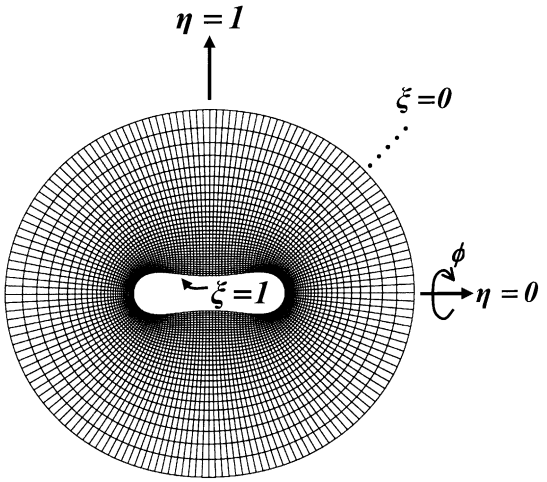

Fig. 3. The orthogonal curvilinear coordinate system around a deformed bubble.

$$\left(\frac{\partial\omega}{\partial t}\right)_{x,\sigma}+\frac{1}{h_\eta h_\xi}\left[\frac{\partial\psi}{\partial\xi}\frac{\partial}{\partial\eta}\left(\frac{\omega}{\sigma}\right)-\frac{\partial\psi}{\partial\eta}\frac{\partial}{\partial\xi}\left(\frac{\omega}{\sigma}\right)\right]$$
$$=\frac{1}{Re}L^2(\omega\sigma)+\frac{N}{h_\eta h_\xi}\left[h_\xi\frac{\partial F_\eta}{\partial\xi}+F_\eta\frac{\partial h_\eta}{\partial\xi}-h_\xi\frac{\partial F_\xi}{\partial\eta}-F_\xi\frac{\partial h_\xi}{\partial\eta}\right], \tag{27}$$

$$L^2\psi=\omega, \tag{28}$$

where the operator L^2 is defined by

$$L^2=\frac{1}{h_\xi h_\eta}\left[\frac{\partial}{\partial\xi}\left(\frac{f}{\sigma}\frac{\partial}{\partial\xi}\right)+\frac{\partial}{\partial\eta}\left(\frac{1}{\sigma f}\frac{\partial}{\partial\eta}\right)\right], \tag{29}$$

and h_ξ and h_η are the scale factors defined by

$$h_\xi=\left[\left(\frac{\partial x}{\partial\xi}\right)^2+\left(\frac{\partial\sigma}{\partial\xi}\right)^2\right]^{1/2},\quad h_\eta=\left[\left(\frac{\partial x}{\partial\eta}\right)^2+\left(\frac{\partial\sigma}{\partial\eta}\right)^2\right]^{1/2}, \tag{30}$$

and $f(\xi,\eta)$ is the distortion factor defined as $f=h_\eta/h_\xi$.

In (27) and (28), ω is the $\mathbf{e}_\phi$-component of the vorticity vector $\boldsymbol{\omega}=\nabla\times\mathbf{u}$ and the stream-function ψ is defined so as to satisfy

$$u_\xi=-\frac{1}{\sigma h_\eta}\frac{\partial\psi}{\partial\eta},\quad u_\eta=\frac{1}{\sigma h_\xi}\frac{\partial\psi}{\partial\xi}. \tag{31}$$

F_ξ and F_η in (28) are the components of the Lorentz force in ξ- and η-directions and they are given by

$$F_\xi=\frac{1}{h_\eta^2\sigma}\frac{\partial x}{\partial\eta}\left[\frac{1}{h_\eta}\frac{\partial\psi}{\partial\eta}\frac{\partial x}{\partial\eta}-\frac{1}{h_\xi}\frac{\partial\psi}{\partial\xi}\frac{\partial\sigma}{\partial\eta}\right], \tag{32}$$

$$F_\eta = \frac{1}{h_\eta^2 \sigma}\frac{\partial \sigma}{\partial \eta}\left[\frac{1}{h_\eta}\frac{\partial \psi}{\partial \eta}\frac{\partial x}{\partial \eta} + \frac{1}{h_\xi}\frac{\partial \psi}{\partial \xi}\frac{\partial \sigma}{\partial \eta}\right]. \tag{33}$$

The boundary conditions in terms of ω and ψ are: at far field

$$\omega \to 0 \quad \text{and} \quad \psi \to \frac{1}{2}x\sigma^2 \quad \text{as} \quad \xi \to 0, \tag{34}$$

and at the gas–liquid interface we require

$$\psi = \int_0^\eta (-u_\xi)\sigma h_\eta \, \mathrm{d}\eta = \int_0^\eta \left(-\frac{1}{|\nabla F|}\frac{\partial F}{\partial t}\right)\sigma h_\eta \, \mathrm{d}\eta \quad \text{at} \quad \xi = 1 \tag{35}$$

corresponding to the kinematic condition. In addition, the vorticity at the bubble surface is given by

$$\omega = -\frac{2}{h_\eta}\frac{\partial u_\xi}{\partial \eta} - 2\kappa_{(\eta)}u_\eta \quad \text{at} \quad \xi = 1, \tag{36}$$

where $\kappa_{(\eta)}$ is the normal curvature of the interface in η-direction. In deriving the above condition, the vanishing shear stress condition has been used. The normal stress condition is given by

$$\tau_{\xi\xi} - \frac{1}{W}(\kappa(\eta) + \kappa(\phi)) = 0, \tag{37}$$

where $\kappa_{(\phi)}$ is the normal curvature in the ϕ-direction, and W is the Weber number defined as

$$W = \frac{\rho(E_0 a_0)^2 a_0}{\gamma}. \tag{38}$$

In (37), $\tau_{\xi\xi}$ is the total normal stress, which includes both the pressure and viscous stress contributions and it is given by

$$\tau_{\xi\xi} = -p + \frac{2}{Re}E_{\xi\xi} = -p + \frac{2}{Re}\left[\frac{1}{h_\xi}\frac{\partial u_\xi}{\partial \xi} + \frac{u_\eta}{h_\xi h_\eta}\frac{\partial h_\xi}{\partial \eta}\right], \tag{39}$$

where $E_{\xi\xi}$ is the component of the rate of strain tensor. Finally, in order to remove the singularity in ψ as $\xi \to 0$, we define

$$\psi^* \equiv \psi - \frac{1}{2}x\sigma^2(1 - \xi^5), \tag{40}$$

which is bounded as $\xi \to 0$.

The governing equations for the grid generation and the flow field can be expressed in the following standard form after discretization:

$$f^2\frac{\partial^2 w}{\partial^2 \xi} + \frac{\partial^2 w}{\partial^2 \eta} + q_1\frac{\partial w}{\partial \xi} + q_2\frac{\partial w}{\partial \eta} + q_3 w + q_4 = 0, \tag{41}$$

where w stands for a general dependent variable, which may be x, σ, ω, ψ^*. In Table 1, q_i are shown for ψ^* and ω. Except for the coefficients q_i, all the detailed numerical steps are more or less the same as those in Kang and Leal (1987). (So any interested readers are recommended to refer to the paper.) In all computations, 41×41 grid system has been used. For unsteady computations,

Table 1
The coefficients q_i in Eq. (41)

w	q_i
ψ^*	$q_1 = f\dfrac{\partial f}{\partial \xi} - \dfrac{f^2}{\sigma}\dfrac{\partial \sigma}{\partial \xi}$
	$q_2 = -\dfrac{1}{f}\dfrac{\partial f}{\partial \eta} - \dfrac{1}{\sigma}\dfrac{\partial \sigma}{\partial \eta}$
	$q_3 = 0$
	$q_4 = -\dfrac{1}{2}\left(20f\sigma x\xi^3 + 15fx\xi^4\dfrac{\partial \sigma}{\partial \xi} + 5\sigma x\xi^4\dfrac{\partial f}{\partial \xi} + 10f\sigma\xi^4\dfrac{\partial x}{\partial \xi}\right)(f\sigma) - h_\eta^2\sigma\omega$
ω	$q_1 = f\dfrac{\partial f}{\partial \xi} + \dfrac{f^2}{\sigma}\dfrac{\partial \sigma}{\partial \xi} - Re\,fh_\eta u_\xi - Ref\left(\dfrac{\partial \sigma}{\partial \eta}\right)\left(\dfrac{\partial x}{\partial t}\right)_{\xi,\eta} + Ref\left(\dfrac{\partial x}{\partial \eta}\right)\left(\dfrac{\partial \sigma}{\partial t}\right)_{\xi,\eta}$
	$q_2 = \dfrac{1}{\sigma}\dfrac{\partial \sigma}{\partial \eta} - \dfrac{1}{f}\dfrac{\partial f}{\partial \eta} - Re\,h_\eta u_\eta + Ref\left(\dfrac{\partial \sigma}{\partial \xi}\right)\left(\dfrac{\partial x}{\partial t}\right)_{\xi,\eta} + Ref\left(\dfrac{\partial x}{\partial \xi}\right)\left(\dfrac{\partial \sigma}{\partial t}\right)_{\xi,\eta}$
	$q_3 = -\left(\dfrac{f}{\sigma}\dfrac{\partial \sigma}{\partial \xi}\right)^2 - \left(\dfrac{1}{\sigma}\dfrac{\partial \sigma}{\partial \eta}\right)^2 + Re\,fh_\eta\dfrac{u_\xi}{\sigma}\dfrac{\partial \sigma}{\partial \xi} + Re\,h_\eta\dfrac{u_\eta}{\sigma}\dfrac{\partial \sigma}{\partial \eta} - \dfrac{Re\,fh_\xi h_\eta}{\Delta t}$
	$q_4 = ReNf\left(h_\eta\dfrac{\partial F_\eta}{\partial \xi} + F_\eta\dfrac{\partial h_\eta}{\partial \xi} - h_\xi\dfrac{\partial F_\xi}{\partial \eta} - F_\xi\dfrac{\partial h_\xi}{\partial \eta}\right) + \dfrac{Re\,fh_\xi h_\eta}{\Delta t}\omega^n$

as in Kang and Leal, the fully implicit scheme has been adopted to ensure the stability and the dimensionless step size ranges from $O(10^{-2})$ to $O(10^{-1})$.

5. Results and discussion

We first considered steady-state problems in order to determine the steady bubble shapes as functions of the Reynolds number (Re), the Weber number (W), and the magnetic interaction parameter (N). Our special attention has been paid to the critical phenomena such as the existence of the critical Weber number, beyond which no steady-state solution can be found for fixed Re and N. Then we considered the full unsteady problem to see what the non-existence of steady solution means.

Before going on to the detailed discussion on the results, let us first take a look at typical values of dimensionless parameters. In Table 2, typical values of the four dimensionless parameters N, Re, W, and Re_m are shown for a bubble in molten steel. As we can see in the table, Re_m is very small for all cases and we may neglect the effect as mentioned before.

5.1. The steady-state problem

5.1.1. The effects of uniform magnetic field on the flow field around a spherical bubble

As a preliminary step, we considered the effects of a uniform magnetic field on the flow field around a spherical bubble. We were interested in the change of the normal stress distribution over

Table 2
The typical values of the dimensionless parameters for a bubble in molten steel

	N		Re		W		Re_m	
E_0 (s^{-1}) / $a_0(m)$	10	100	10	100	10	100	10	100
10^{-3}	10	1	10	10^2	4.1×10^{-4}	4.1×10^{-2}	8.8×10^{-6}	8.8×10^{-5}
10^{-2}	10	1	10^3	10^4	4.1×10^{-1}	4.1×10	8.8×10^{-4}	8.8×10^{-3}

$\mu = 12.6 \times 10^{-7}$ H m^{-1}, $\nu = 10^{-6}$ m^2 s^{-1}, $\rho = 7 \times 10^3$ kg m^{-3}, $\gamma = 1.7$ N m^{-1}, $\sigma_c = 0.7 \times 10^6$ Ω^{-1} m^{-1}, $B = 1$ T.

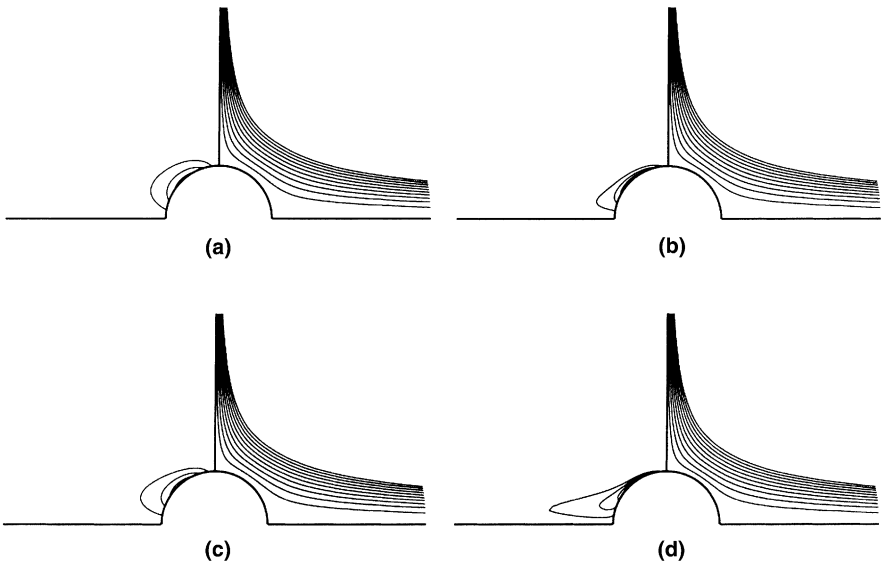

Fig. 4. The effect of magnetic field on the vorticity (left contours in each figure) and streamfunction distributions around a spherical bubble: (a) $Re = 5.0$, $N = 0.0$; (b) $Re = 50$, $N = 0.0$; (c) $Re = 5.0$, $N = 2.0$; (d) $Re = 50$, $N = 2.0$.

the bubble surface due to the flow field change. One set of results is shown in Fig. 4, where the vorticity and the streamfunction distributions are shown. Compared with the vorticity distributions, the convection effect becomes dominant when the magnetic field is present. This effect is apparently similar to the velocity increase near the bubble. This behavior may be explained as follows.

As well known, the uniform static magnetic field acts as a brake for the fluid motion. In the preliminary analysis section, we have seen that the pressure field must be changed in order to overcome this braking effect. We have higher pressure near the equatorial plane. The braking force per unit volume of fluid is proportional to the velocity component that is orthogonal to the imposed magnetic field ($F \propto u_\perp$). If there is no bubble, the velocity field would be linear and the pressure field would follow the expression in the preliminary analysis section. This modified pressure field balances the braking effect to keep the velocity unchanged. However, the existence of a bubble causes a change. Near the bubble surface, where the flow is mainly directed parallel to the magnetic field lines, the braking effect diminishes. Thus, the flow is more accelerated near the bubble surface compared with the no magnetic field case. This may explain the observed numerical results.

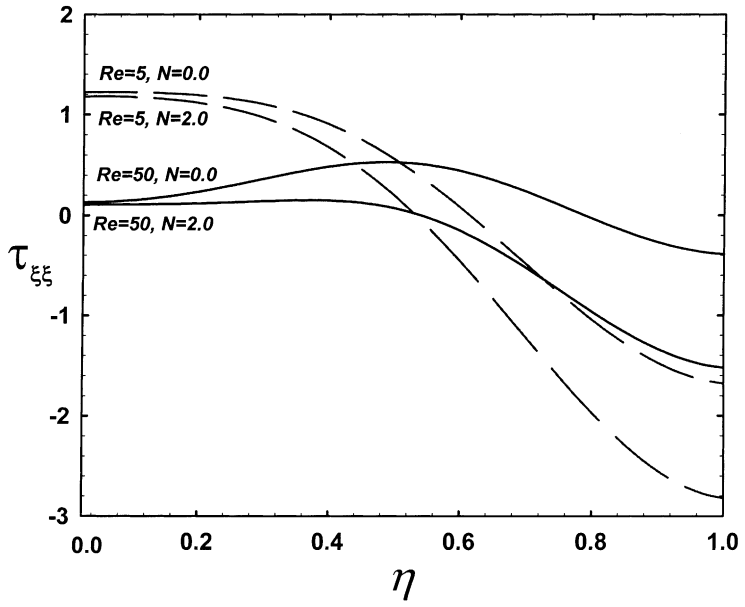

Fig. 5. The distribution of normal stress $\tau_{\xi\xi} = -p + (2/Re)E_{\xi\xi}$ at the surface of a spherical bubble ($\eta = 0$ corresponds to the rotation axis and $\eta = 1$ corresponds to the equatorial plane of the bubble).

In order to predict the effects of magnetic field on the steady bubble shape under the condition that the far field velocity is unchanged, we plot the normal stress

$$\tau_{\xi\xi} = -p + \frac{2}{Re}E_{\xi\xi}$$

along the spherical bubble surface in Fig. 5. In the figure, $\eta = 0$ corresponds to the rotation axis and $\eta = 1$ to the equatorial plane (in the case of a spherical bubble, $\theta = (\pi/2)\eta$). The surface point tends to be pulled outward if $\tau_{\xi\xi}$ is positive, while pushed inward if negative. Since we need to consider the constant volume constraint, the above argument should be modified for the relative values to a certain mean value. When we compare the results for $N = 0$ and $N = 2.0$ at $Re = 5$, we can see that under the magnetic field the bubble surface is expected to be more pulled outward near the rotation axis and more pushed inward near the equatorial plane. Consequently, it is expected to have more elongation of a bubble under the magnetic field. When $Re = 50$ and $N = 0$, the normal stress has maximum value near $\eta = 0.5$. This is because of the pressure field that tends to follow the Bernoulli's principle as the Reynolds increases. Even for this high Reynolds number case, we can see that under the magnetic field the bubble is expected to be somewhat elongated in the rotational axis direction. The effects of magnetic field on the steady shape of a bubble will be shown shortly in the following section.

Before going on to the detailed discussion, it should be mentioned that, the Reynolds number and the Weber number are defined differently from those of Ryskin and Leal (1984b), and Kang and Leal (1987). There is a factor of 2 between theirs and the present paper.

When a magnetic field is applied, the steady-state shapes are determined by the three parameters, Re, W, and N. On the other hand, in the case of no magnetic field, the bubble shape is characterized by the two dimensionless parameters, Re and W. For the bubble deformation in a

uniaxial straining flow, Ryskin and Leal (1984b) indicated that there exists a critical W_c, for $Re \geqslant 5$, which is a limit point on the branch of steady solutions that begins with the spherical solution at $W = 0$. Physically, the limit point seems to correspond to the first appearance of a waist in the prolate shapes that were obtained by Kang and Leal (1987). The waist in a prolate bubble means that the deformed bubble shape has negative η-directional curvature near the equatorial plane, $\kappa(\eta) < 0$. This has been believed to be an indicator of bubble breakup in the case of no magnetic field. Now, we want to see the effect of the magnetic field on the bubble deformation. A special attention will be given to the breakup behavior.

5.1.2. The effects of uniform magnetic field on the steady bubble deformation

The shape of a bubble is determined by the normal stress distribution. Therefore, the general behavior of bubble deformation in a magnetic field can be predicted by looking at the normal stress distribution over the spherical bubble surface. As we have seen in Fig. 5, the magnetic field has an effect of increasing the difference between normal stresses at the pole and the equator ($\tau_{\xi\xi}|_{\eta=0} - \tau_{\xi\xi}|_{\eta=1}$). This means that the pole is more pulled out as the magnetic field effect increases. In order to study the bubble deformation behavior in more detail, the full free boundary problems have been solved and the steady bubble shapes are obtained as a function of the magnetic interaction parameter (N) for the fixed Reynolds and Weber numbers.

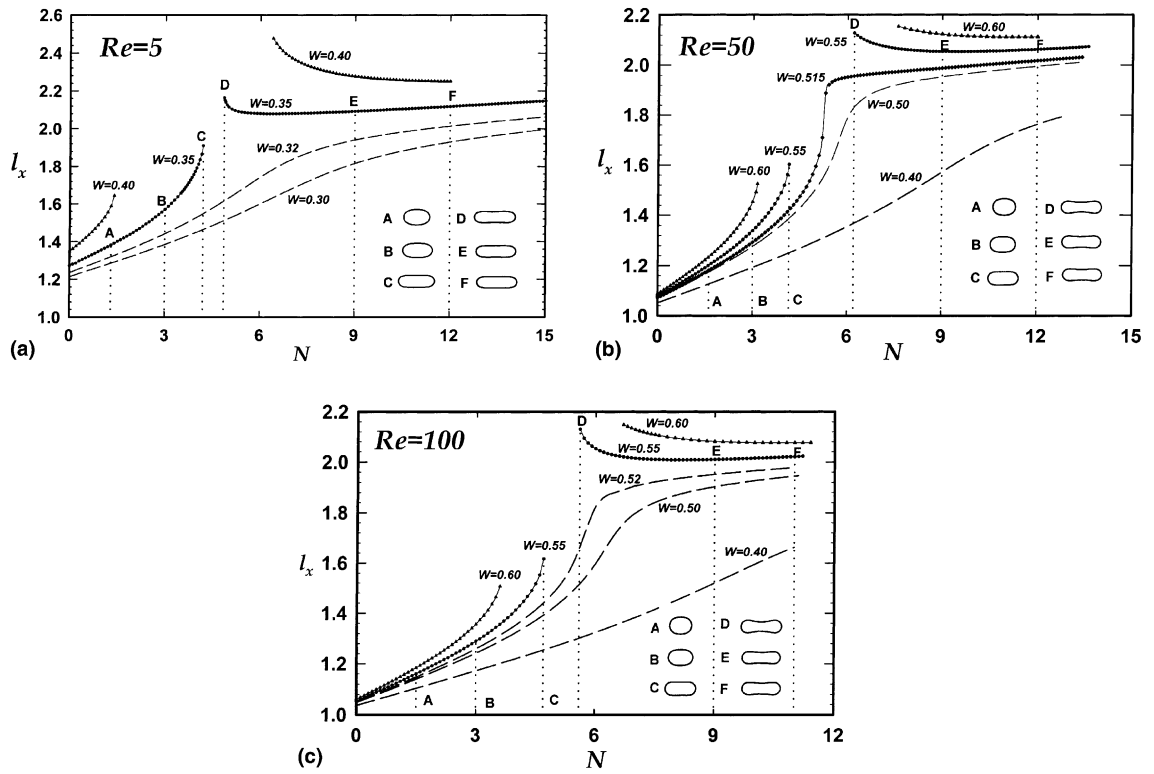

Fig. 6. The steady-state deformation (l_x) of a bubble as a function of the magnetic interaction parameter (N): (a) $Re = 5.0$; (b) $Re = 50$; (c) $Re = 100$.

The results for the $Re = 5$ case are shown in Fig. 6(a). In the figure, l_x is the measure of deformation and defined as the radius along the major axis. As we can see, the bubble deformation increases as N increases for small N. However, when N is increased further with fixed Re and W, the bubble shows distinct deformation behavior depending on the value of W. If W is smaller than a certain threshold value (W_{th}), steady bubble deformation increases monotonously with the increase of N. However, when W is larger than W_{th}, there exist a range of N, $N_{\text{c1}}(W) < N < N_{\text{c2}}(W)$, for which no converged steady-state solution has been obtained. As an example, when $W = 0.35$, the converged steady solution could not be obtained between the points C ($N = 4.2$) and D ($N = 4.86$). It is found that such a critical range of N increases as W increases. The non-existence of the steady solution is believed to be the reason why no converged solution has been obtained for the range $N_{\text{c1}}(W) < N < N_{\text{c2}}(W)$. This fact will be verified by the full unsteady code. In the figure, the steady bubble shapes are shown for several points on the solution curves of $W = 0.35$ ($N = 1.3$ for the point A; 3.0 for B; 4.2 for C; 4.86 for D; 9 for E; 12 for F). The largely deformed shapes at D, E, and F have the negative curvature in η-direction. As discussed earlier, if there were no magnetic field, such steady bubble shapes with $\kappa_{(\eta)} < 0$ would not be possible. In that sense, this is an interesting deformation characteristics in magnetic field. This point will be discussed later in detail.

Similar deformation behavior has been observed for the cases of $Re = 50$ and $Re = 100$. In the case of $Re = 50$, the steady bubble shapes for several points on the solution curves of $W = 0.55$ are shown ($N = 1.62$ for A; 3.0 for B; 4.15 for C; 6.2 for D; 9 for E; 12 for F). The steady shapes on the points of solution curves of $W = 0.55$ are shown also for the $Re = 100$ case ($N = 1.5$ for A; 3.0 for B; 4.7 for C; 5.6 for D; 9 for E; 11 for F).

The lower critical value of N_{c1} is believed to be a tangential bifurcation point. Since the bubble is deformed more easily as the Weber number increases, for $W > W_{\text{th}}$ the bubble reaches a tangential critical point as shown in the figure. The deformation behavior of a bubble for $W > W_{\text{th}}$ suggests the so-called Whitney pleat in the catastrophe theory (Arnold, 1986). We have tried all possible measures to obtain the solution curves between the lower and the upper critical points, but no converged solution could be obtained with the steady code used in the present work. From the analysis, we obtained one unexpected result. That is the fact that the deformation of bubble does not necessarily increase with the increase of N for the second solution curves of $W > W_{\text{th}}$ (e.g. $W = 0.55$ curve with the points D, E, and F). Unfortunately, however, we are not able to find any suitable explanation to this behavior at this moment.

Now we need to explain the observation of steady bubble shapes with negative η-directional curvature near equatorial plane. As mentioned before, if there were no magnetic field, the bubble could not attain the steady bubble shape with $\kappa_\eta < 0$. If $W > W_{\text{c}}$ (i.e. if the deforming force is larger than a certain limit), the bubble would be elongated indefinitely. Consequently, the radius of bubble on the equatorial plane decreases with the bubble elongation. This means the normal stress is negative (compared with the average value) near the equatorial plane. However, under the magnetic field, steady bubble shape with negative η-directional curvature is possible as we have seen above. In order to have such a steady bubble shape, the relative normal stress near the equatorial plane should be less negative compared with the case of no magnetic field. Along the equatorial plane, the incoming flow is orthogonal to the magnetic field and the flow is most decelerated by the magnetic damping effect. Therefore, the relative normal stress at the bubble surface near the equatorial plane becomes less negative (negative normal stress means that the

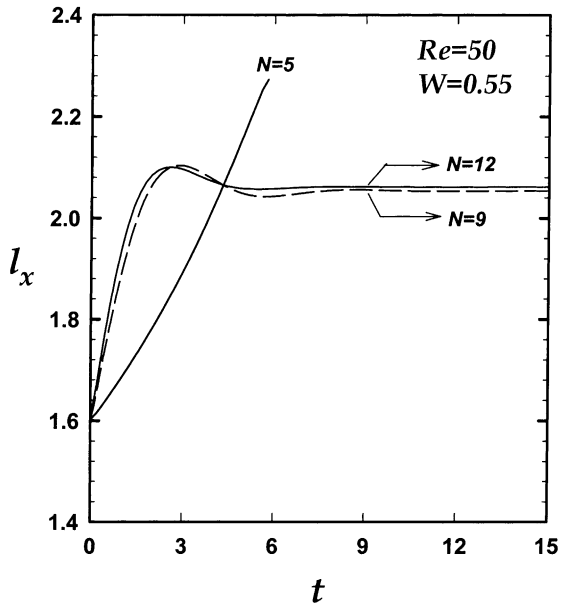

Fig. 7. Unsteady deformation characteristics of a bubble with $Re = 50$, $W = 0.55$.

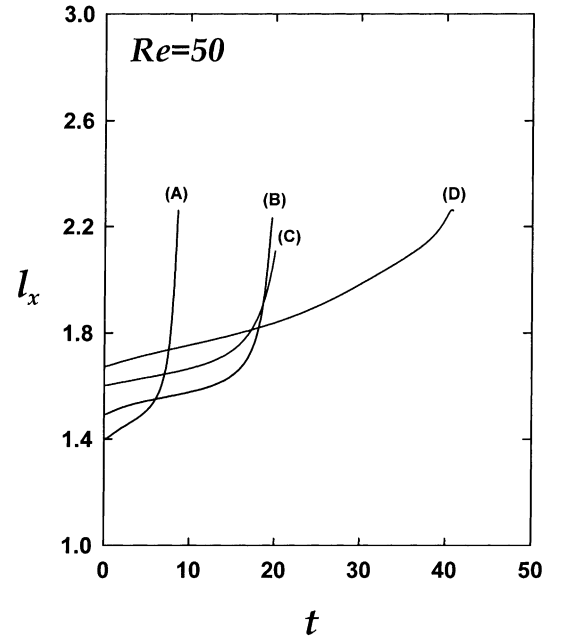

Fig. 8. The unsteady bubble deformations at slightly supercritical N (with respect to N_{c1}) when $Re = 50$: (A) $W = 0.75$, $N = 1.50$ ($N_{c1} = 1.40$); (B) $W = 0.6$, $N = 3.20$ ($N_{c1} = 3.15$); (C) $W = 0.55$, $N = 4.20$ ($N_{c1} = 4.15$); (D) $W = 0.52$, $N = 5.10$ ($N_{c1} = 5.00$).

surface force is inward and the bubble surface is pushed inward). The above mechanism may explain the interesting steady bubble shape.

5.2. The unsteady-state problem

From the studies on the steady bubble deformation, it has been suggested that if $W > W_{th}$ there exists a certain critical range of N, $N_{c1}(W) < N < N_{c2}(W)$, for which no steady solution has been found. On the other hand, if $W < W_{th}$, it has been found that the steady deformation increases monotonously as N increases. In the present section, we want to confirm the findings from the steady analysis by solving the full unsteady problem. For simplicity in the analysis, we choose one value of the Reynolds number $Re = 50$.

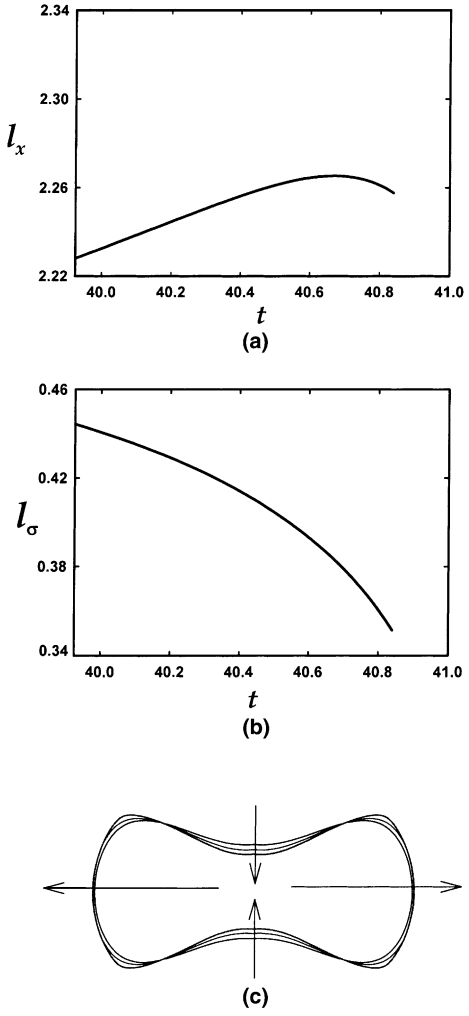

Fig. 9. The unsteady bubble deformation when $Re = 50$, $W = 0.52$, and $N = 5.1$: (a) major axis; (b) minor axis; (c) consecutive unsteady bubble shapes at $t = 40.0$, $t = 40.6$, and $t = 40.84$.

5.2.1. The existence of critical range, $N_{c1}(W) < N < N_{c2}(W)$

From the results of steady analysis shown in Fig. 6, it has been found that for $W > W_{th}$ there exists a certain critical range of N in which no converged steady solution could be obtained. We assume that no converged solution means true non-existence of steady solution in the critical range. In this section, we want to confirm our assertion by the full unsteady analysis.

To do that we considered the $Re = 50$ case and performed full unsteady analysis. As the initial condition, we chose the steady solution at the point C ($W = 0.55$ and $N = 4.15$). At $t = 0$ we suddenly increased the N values to 5, 9, and 12. $N = 5$ is in the critical range, but at other N values steady solutions exist as shown in Fig. 6(b). The results for the unsteady deformation are shown in Fig. 7. For small t, the bubble is elongated in every case. However, long time behavior is quite different. As expected, when $N = 9$ and $N = 12$, the bubble reaches the steady states after some overshoots. However, the bubble is elongated indefinitely at $N = 5$ in the critical range. Therefore, we can see that no converged steady solution in the critical range implies indefinite deformation in unsteady dynamics.

In order to better understand the meaning of the critical range of N, we have performed further unsteady computations at slightly supercritical N (with respect to N_{c1}) values for $W = 0.75$, $W = 0.60$, $W = 0.55$, and $W = 0.52$ cases when $Re = 50$. The results are shown in Fig. 8. We begin with the steady solutions at the lower critical value of N: $N_{c1} = 1.40$ for $W = 0.75$ (curve A), $N_{c1} = 3.15$ for $W = 0.60$ (curve B), $N_{c1} = 4.15$ for $W = 0.55$ (curve C), and $N_{c1} = 5.00$ for $W = 0.52$ (curve D). Then at $t = 0.0$, we suddenly change N to the slightly supercritical values ($N = 1.50$ for $W = 0.75$, $N = 3.20$ for $W = 0.60$, $N = 4.20$ for $W = 0.55$, and $N = 5.10$ for $W = 0.52$) and follow the subsequent deformations of the bubble. Fig. 8 indicates the elongation of a bubble without limit eventually leading to bubble breakup in unsteady state. To make sure that the deformations in Fig. 8 lead to eventual breakup, we examine the case of $Re = 50$ and $W = 0.52$ (curve D), which shows relatively slow elongation compared with others. We plot l_x and l_σ in Fig. 9 near $t = 40$, where l_σ is the radius of a bubble at the equatorial plane. From the figures, we can see that l_y drops rapidly and this suggests that the bubble breakup will occur.

The solution of the soap film problem may provide another insight. We may consider two bubble radii at two different points on the axis. One is $l_{\sigma 1}$ at $x = 0$ which is the minimum radius in σ-direction, and the other is $l_{\sigma 2}$ at $x = x_0$ which has maximum value (see Fig. 10(a)). The time-dependent curve of $l_{\sigma 1}/l_{\sigma 2}$ in Fig. 10(b) shows a steep decrease and it is another indicator of breakup. The soap film problem is of course different from the bubble breakup problem in various aspects. However, from the soap film problem, we may get some insight on breakup. In the problem of a soap film hanged between two rings of unit radius, the soap film is broken up automatically (Arfken, 1970) if the radius at the center point ($x = 0$) is smaller than 0.5524.

5.3. Stability diagram

Now, the numerical results from steady and unsteady analyses are summarized. The shape of a bubble is a function of three dimensionless parameters: the Reynolds number (Re), the Weber number (W), and the magnetic interaction parameter (N). Summarizing the numerical results, the stability diagram is prepared and shown in Fig. 11. For each Reynolds number, the critical Weber number for bubble breakup (W_c) decreases as the magnetic interaction parameter N increases. However, this decreasing behavior is limited by a threshold value of W and the breakup behavior

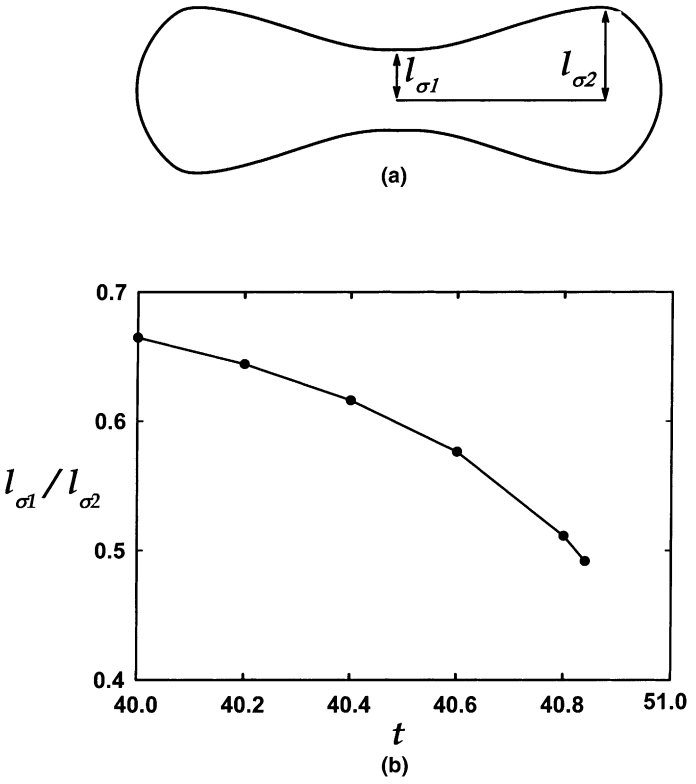

Fig. 10. The ratio of the minimum l_σ to the maximum l_σ for a bubble with a waist near the equatorial plane when $Re = 50$, $W = 0.52$, and $N = 5.1$.

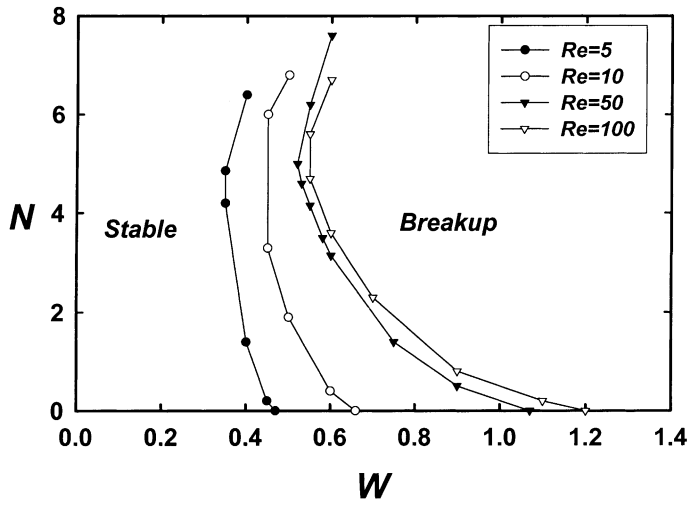

Fig. 11. The stability diagram of a bubble as a function of Re, W, and N.

has been observed only for $W > W_{th}$. Further increase of N stabilizes the bubble dynamics and W_c increases with N. Therefore, for fixed Re and $W > W_{th}$, we have a critical range, $N_{c1}(W) < N < N_{c2}(W)$, for bubble breakup.

In the present study, we have considered the cases of $Re \leqslant 100$. For larger Reynolds numbers, the bubble behavior is expected to be more or less the same as in the case of $Re = 100$. When there is no magnetic field effect, Ryskin and Leal (1984b) obtained $W_c = 1.35$ (in their notation $W_c = 2.7$) for the potential flow case. This fact partly justifies our assertion. For small $W < W_{th}$, the breakup has not been observed at least in the range of parameters considered in the present study.

With the diagram, the maximum allowable size can be estimated for a bubble in a linear flow under the uniform magnetic field. For this purpose the following relation may be used:

$$W = \frac{\rho E_0^2 a_0^3}{\gamma} < W_c.$$

By estimating E_0 of the flow field near the bubble, we may compute N first with the given ρ, σ_c, and B_c (see Eq. (13)). Assuming a large Reynolds number, we can read the value of W_c from the diagram (say, the curve for $Re = 100$). Then, by using the above relation, the maximum bubble size can be estimated. If the Reynolds number is not so large, a few iterations may be needed.

6. Conclusion

In order to investigate the effects of a uniform magnetic field on the deformation and breakup of a bubble, numerical analyses using the steady and unsteady codes have been performed. For simplicity, we have considered only the magnetic field parallel to the rotation axis of the bubble. From the numerical results, we have reached the following conclusions:

(i) The uniform magnetic field increases the elongation of a bubble in the axial direction if the same far field velocity distribution is assumed as in the case of no magnetic field.

(ii) When the same local rate of strain is assumed near the bubble, the critical Weber number (W_c) for the existence of steady shape decreases as N increases (from $N = 0$) until a certain threshold value (W_{th}) is reached.

(iii) For fixed Re and $W < W_{th}$, the bubble elongation increases monotonously as N increases. However, if $W > W_{th}$, there exists a critical range, $N_{c1}(W) < N < N_{c2}(W)$, for which no converged steady solution has been obtained. By using the full unsteady code, we have shown that the bubble is elongated indefinitely in the critical range of N.

(iv) The numerical results from the present study are summarized in a diagram for the stability and breakup of a bubble in a magnetic field. The diagram is expected to provide some valuable information for estimation of the maximum allowable bubble size in the system.

Acknowledgements

This work has been supported by the grant from the BK21 program of Korean Ministry of Education. The authors greatly appreciate the financial support.

References

Arfken, G., 1970. Mathematical Methods for Physicists, second ed. Academic Press, New York.

Arnold, V.I., 1986. Catastrophe Theory, second ed. Springer, Berlin.

Cho, H.J., Kang, I.S., Kweon, Y.C., Kim, M.H., 1996. Study of the behavior of a bubble attached to a wall in a uniform electric field. Int. J. Multiphase Flow 22, 909–922.

Eckert, S., Gerbeth, G., Lielausis, O., 2000a. The behaviour of gas bubbles in a turbulent liquid metal magnetohydrodynamic flow. Part I: Dispersion in quasi-two-dimensional magnetohydrodynamic turbulence. Int. J. Multiphase Flow 26, 45–66.

Eckert, S., Gerbeth, G., Lielausis, O., 2000b. The behaviour of gas bubbles in a turbulent liquid metal magnetohydrodynamic flow. Part II: Magnetic field influence on the slip ratio. Int. J. Multiphase Flow 26, 67–82.

Jones, T.B., 1978. Electrohydrodynamically enhanced heat ransfer in liquids – a review. Adv. Heat Transfer 14, 107–148.

Kang, I.S., Leal, L.G., 1987. Numerical solution of axisymmetric, unsteady free-boundary problems at finite Reynolds number. I. Finite-difference scheme and its application to the deformation of a bubble in a uniaxial straining flow. Phys. Fluids 30, 1929–1940.

Miksis, M.J., 1981. A bubble in an axially symmetric shear flow. Phys. Fluids 24, 1229–1231.

Moreau, R., 1990. Magnetohydrodynamics. Kluwer Academic Publishers, Dordrecht.

Ryskin, G., Leal, L.G., 1984a. Numerical solution of free-boundary problems in fluid mechanics. Part 1, The finite-difference technique. J. Fluid Mech. 148, 1–17.

Ryskin, G., Leal, L.G., 1984b. Numerical solution of free-boundary problems in fluid mechanics. Part 3, Bubble deformation in an axisymmetric straining flow. J. Fluid Mech. 148, 37–43.

Ryskin, G., Leal, L.G., 1983. Orthogonal mapping. J. Comput. Phys. 50, 71–100.